Supporting Information

Nanoporous high-entropy alloys for highly stable and efficient catalysis

Hua-Jun Qiu,*[a] Gang Fang,[a] Yuren Wen,*[b] Pan Liu,*[c] Guoqiang Xie,[a] Xingjun Liu*[ae] and Shuhui Sun[d]

[a]School of Materials Science and Engineering, Harbin Institute of Technology, Shenzhen, 518055, China
*Email: qiuhuajun@hit.edu.cn; lxj@xmu.edu.cn
[b]School of Materials Science and Engineering, University of Science and Technology Beijing, Beijing 100083, China
*E-mail: wyrcsu@163.com
[c]State Key Laboratory of Metal Matrix Composites, School of Materials Science and Engineering, Shanghai Jiao Tong University, Shanghai 200030, P. R. China
*Email: panliu@sjtu.edu.cn
[d]Institut National de la Recherche Scientifique-Énergie Matériaux et Télécommunications, Varennes, Quebec J3X 1S2, Canada
*E-mail: shuhui@emt.inrs.ca
[e]State Key Laboratory of Advanced Welding and Joining, Harbin Institute of Technology, Shenzhen 518055, China

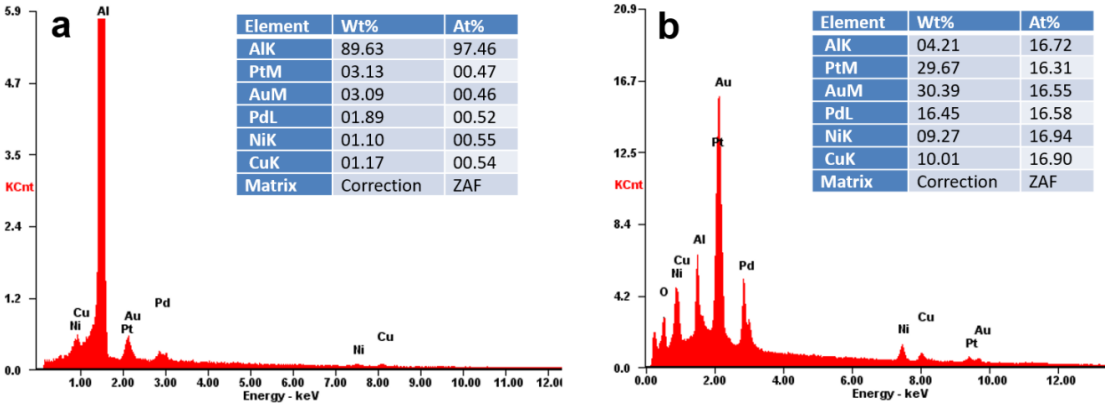

Figure S1. EDS spectra of the senary HEA alloy before (a) and after (b) dealloying in 0.5 M KOH.

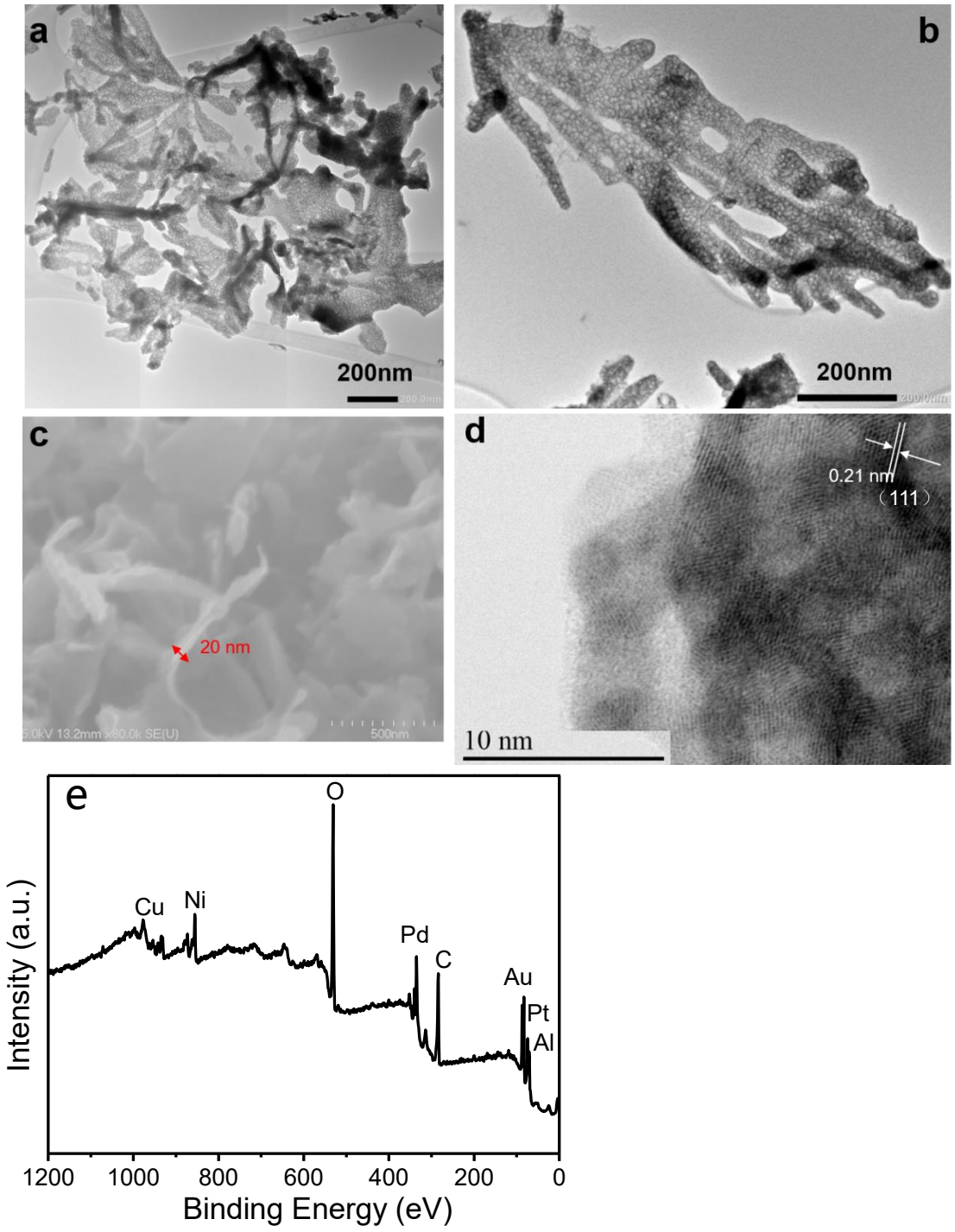

Figure S2. TEM images (a and b), SEM image (c) and bright field STEM image (d) of the np-HEA. XPS scan spectrum of the np-HEA (e).

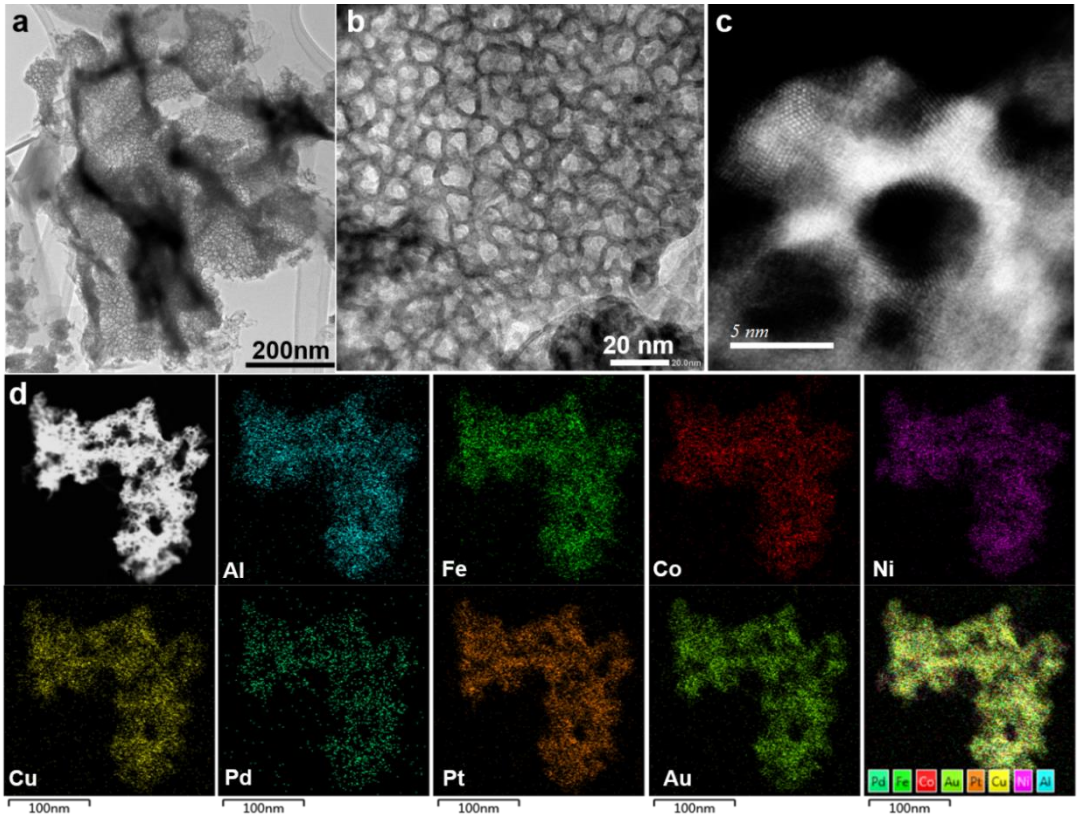

Figure S3. TEM (a and b), HAADF-STEM (c) and EDS mapping (d) of the octonary np-HEA.

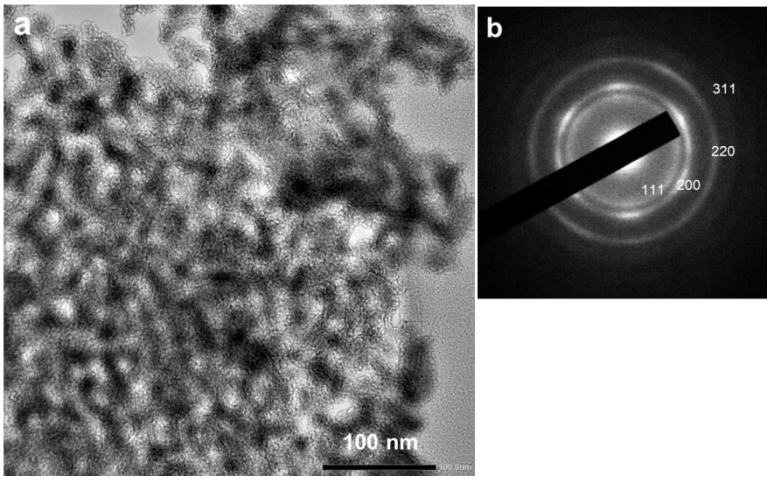

Figure S4. TEM (a) image of np-AlNiCuMoCoFe HEA and the corresponding SAED pattern (b) which is similar to that of np-AlNiCuPtPdAu sample, demonstrating the FCC structure with surface oxides. Due to the highly oxidation of these non-noble metals, the nanopores are filled with (oxy)hydroxides.

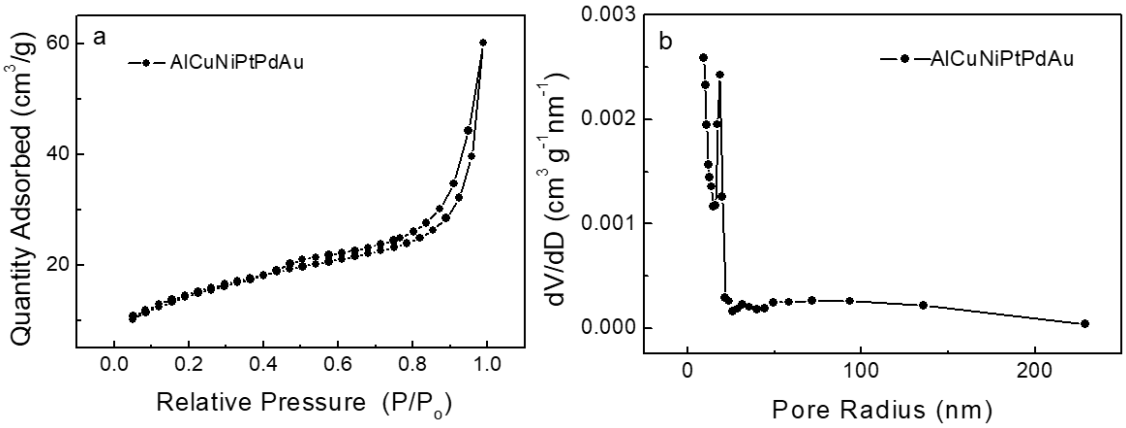

Figure S5. N_2 adsorption–desorption isotherms (a) and pore size distribution (b) of the senary np-HEA.

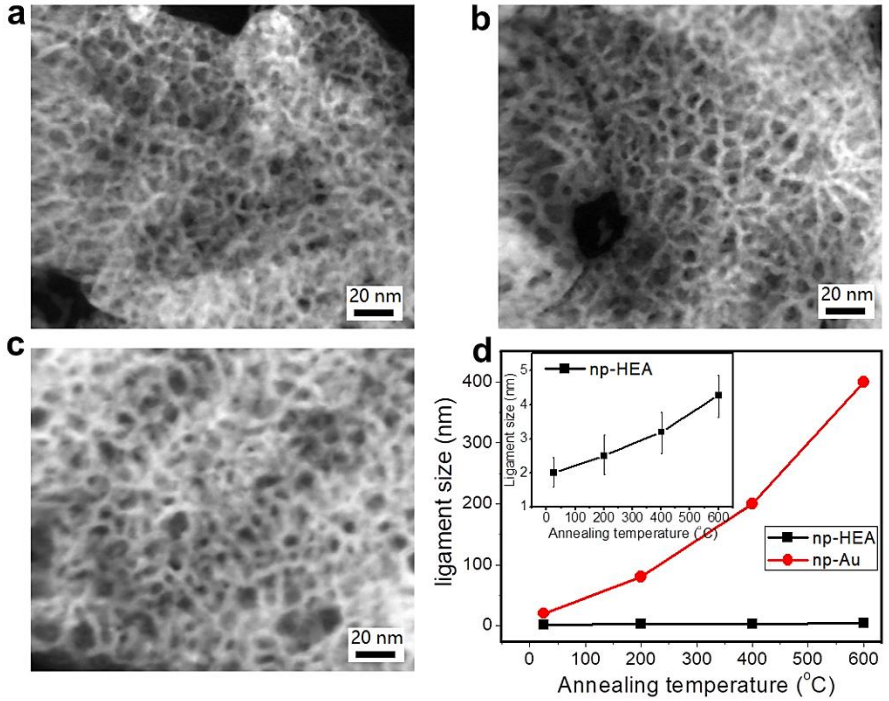

Figure S6. STEM images of the senary np-HEA after annealing at 200 ºC (a), 400 ºC (b), and 600 ºC (c) in N_2 atmosphere for 1 h. (d) is the ligament size change with the annealing temperatures and inset in (d) is the change of ligament size of np-HEA.

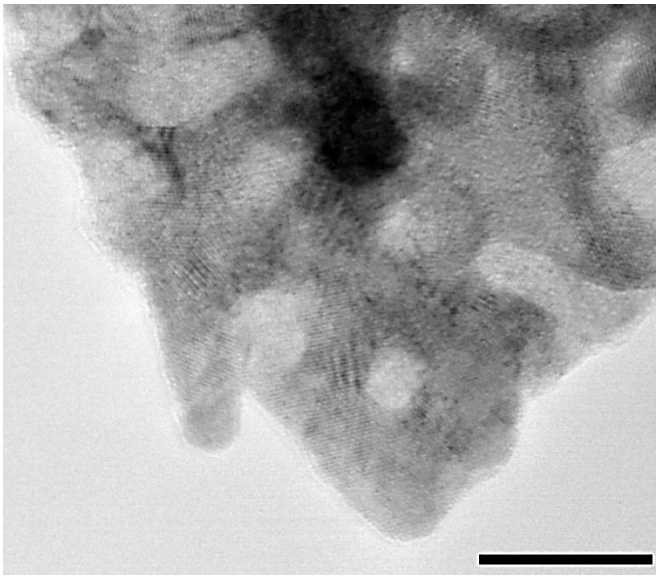

Figure S7. HRTEM image showing the removal of surface oxide layer by acidic etching. Scale bar: 10 nm.

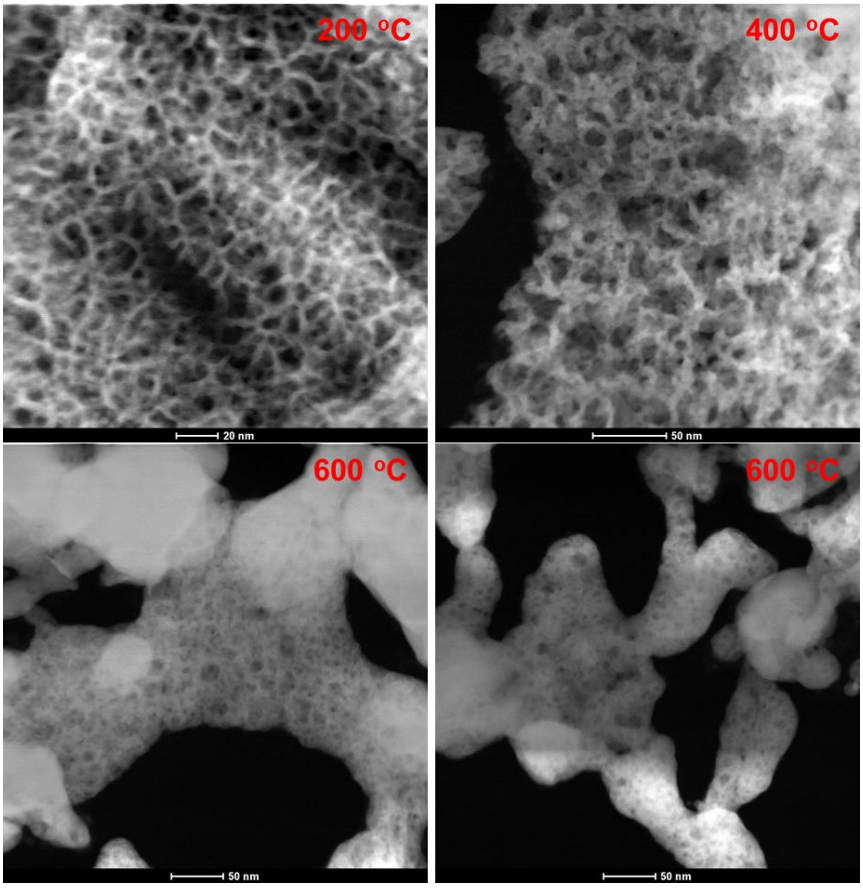

Figure S8. STEM images of the np-HEA without oxides coating after annealing in N_2 atmosphere at different temperatures for 1 h.

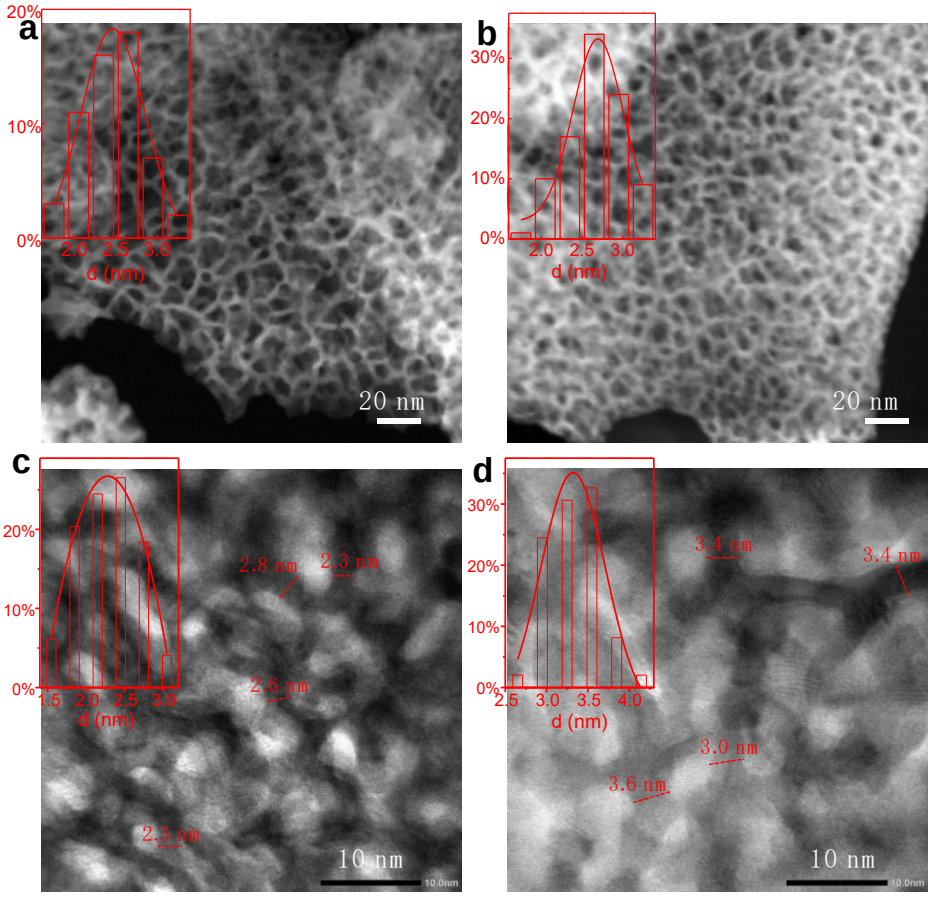

Figure S9. STEM/TEM images of the np-HEA without oxides coating (a and b) and np-Pt (c and d) before (a and c) and after (b and d) 10 h annealing at 200 ºC in N_2 atmosphere. Insets are the ligament size distribution of each samples (50 ligaments are measured).

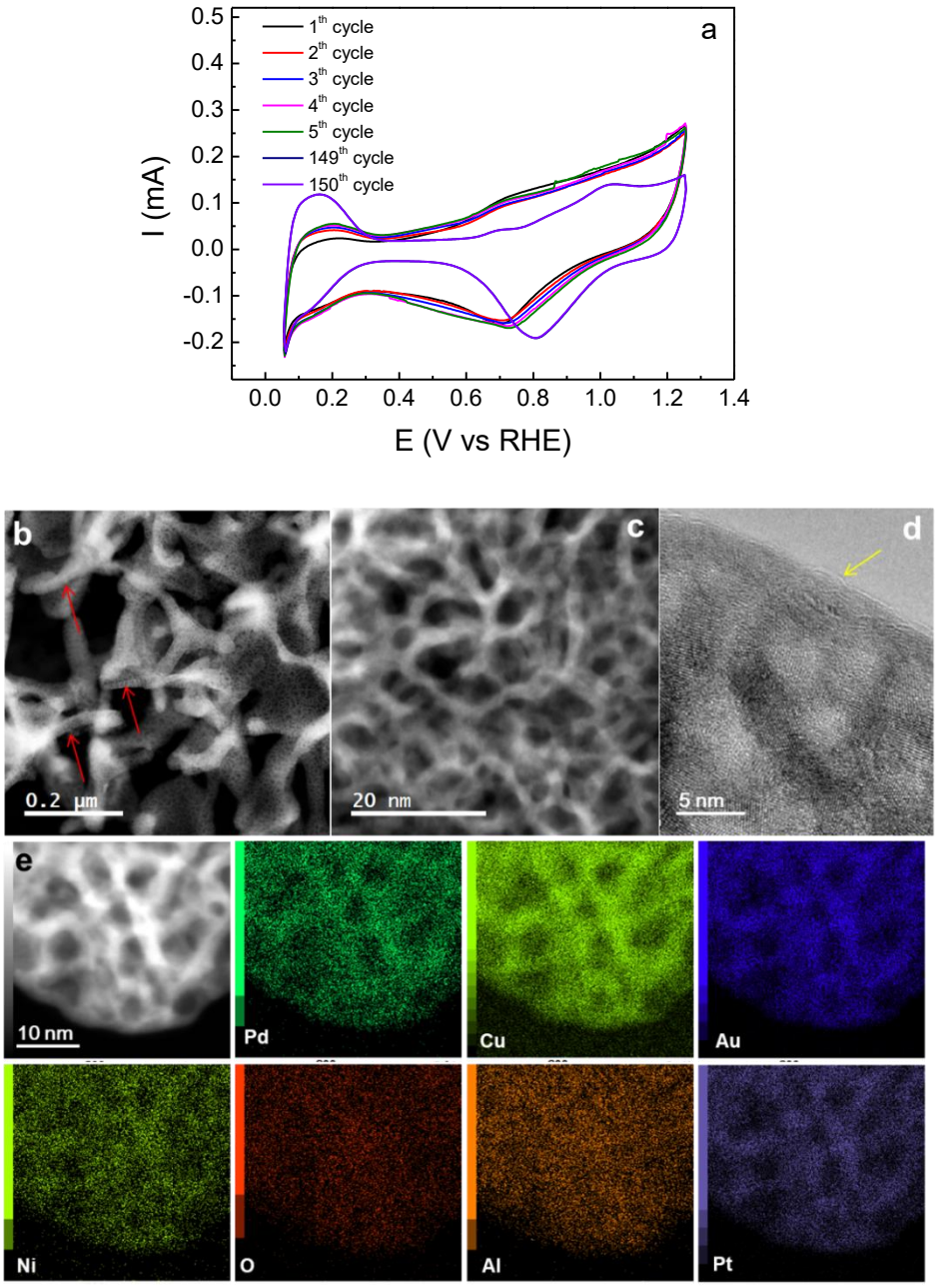

Figure S10. CV curves showing the activation process of the np-HEA in 0.1 M $HClO_4$ solution until it reaches a steady state after 150 cycles (a). STEM images (b: low magnification and c: high magnification), HRTEM image (d) and STEM-mapping (e) of the electrochemical activated np-HEA. The arrows in (b) show the edges of the first-level nanostructure which is very thin (less than 20 nm). The arrow in (d) shows that the oxide coating is basically removed.

a

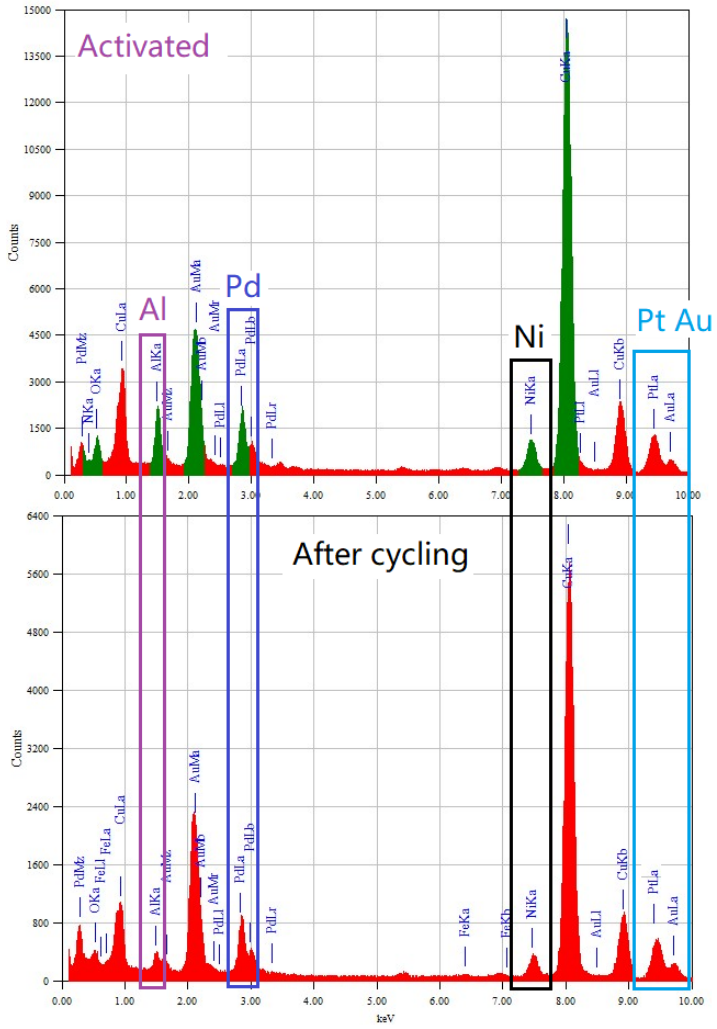

b

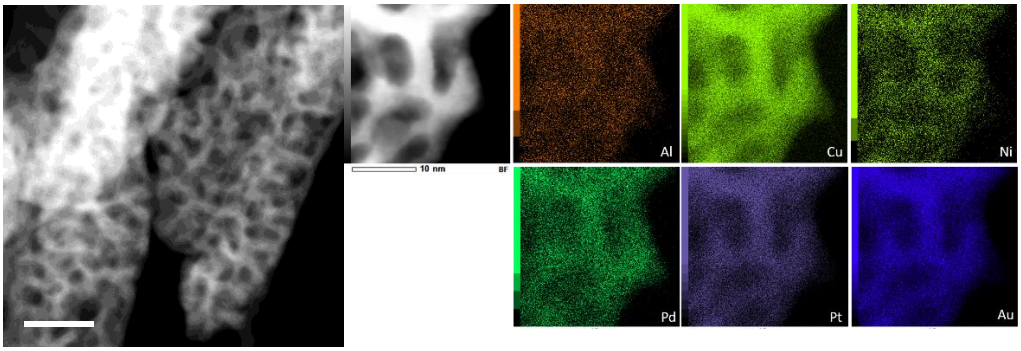

Figure S11. Comparison of the STEM-EDS spectrum of the np-HEA (a). STEM image and EDS-mapping of the np-HEA after long-term electrochemical cycling. The results show the further etching of Al and Ni (slightly) after the cycling. The distribution of the six elements is still very uniform with no element separation. The coarsening of ligaments is not observed.

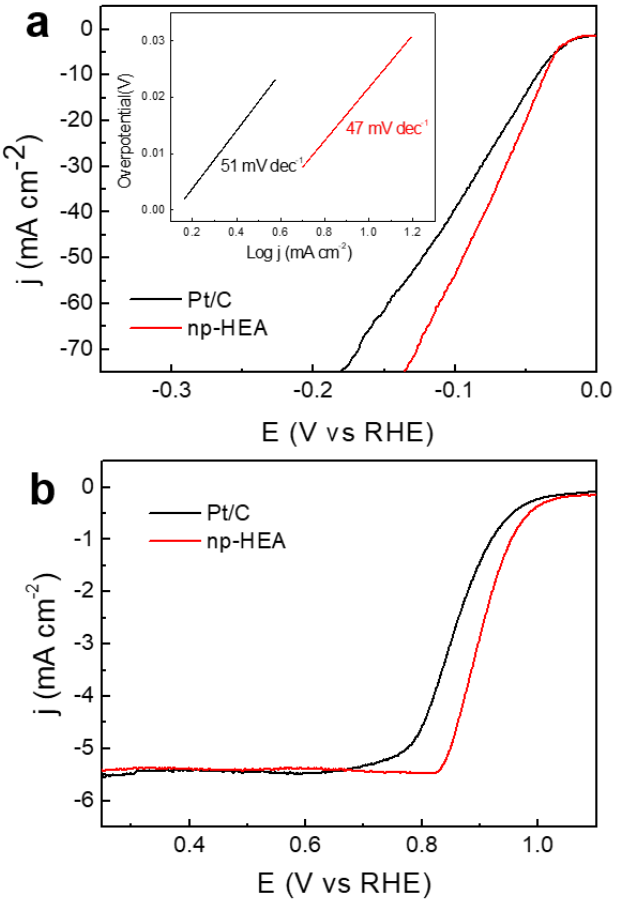

Figure S12. HER (a) and ORR (b) polarization curves of np-HEA and Pt/C in 0.1 M KOH solution. Inset in (a) is the Tafel plot for HER. The high current density and smaller Tafel slope shows the higher catalytic activity for HER. The greatly negatively shifted half-wave potential demonstrates the enhanced ORR activity in alkaline solution.

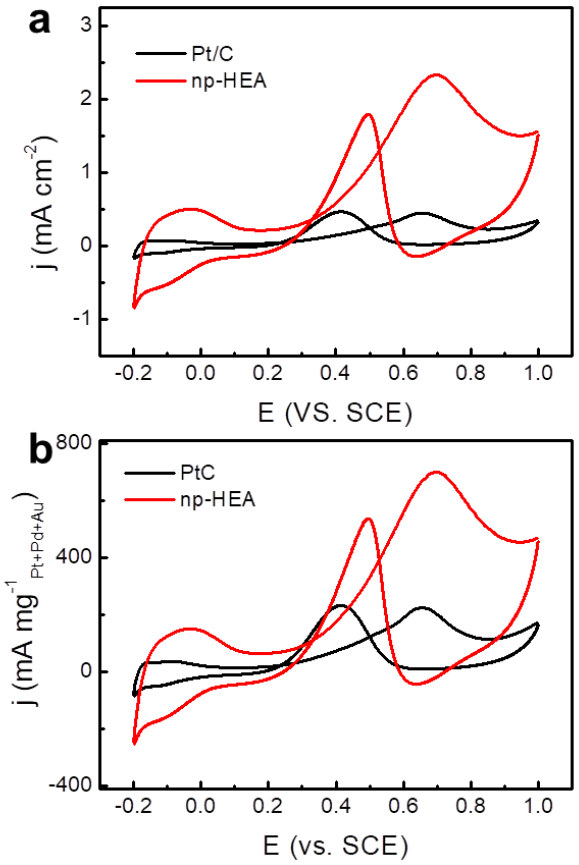

Figure S13. CV curves of the senary np-HEA and Pt/C catalysts in 0.5 M H_2SO_4 + 0.5 M CH_3OH solution. (a) is normalized by the EASA of Pt and (b) is normalized by the mass of Pt+Pd+Au. Scan rate: 50 mV s^{-1}.

Table S1. Comparison of the ORR activity (at 0.9 V) with literature data.

Catalysts	Mass activity ($A\ mg^{-1}_{Pt}$)	Specific activity ($mA\ cm^{-2}$)	References
Pt-Ni NFs/C	2.98	6.37	*Nano Lett. 2016, 16, 2762-2767*
$Pt_{3.3}$/CoO	0.59	2.85	*ACS Appl. Energy Mater. 2018, 1, 1840-1845*
NPG-Pd-Pt	1.63	0.95	*Nature Energy* 2017, 2, 17111
Pt–FeNC	0.69	--	*Chem. Commun.,* 2017, 53, 1660--1663
PtCuAu-8 M	1.45	4.12	*J. Mater. Chem. A*, 2018, 6, 12541–12550
$PtNi_{0.56}Pd_{1.42}$ NWs	1.93	3.48	*Adv. Mater.* 2017, 1603774
Pt_2CuNi/C	2.35	--	*ACS Catal.* 2015, 5, 2296-2300
$Pt_{76}Cu_{24}$	0.466	1.273	*Appl. Catal. B2018,* 236, 359–367.
$PtCu_{2.1}$NPs	1.56	3.31	*Nano Lett. 2016, 16, 5037-5043*
Pt-skin Pt_3Fe NWs/C	2.11	4.34	*Adv. Mater.* 2018, 30, 1705515
PtCu NFs	0.211	1.71	*Adv. Mater.* 2016*,* 28, 8712
Star-shaped AuPt/C	0.89	0.78	*Nano Lett*. 2015, 15, 7808
$PtPb_{1.12}Ni_{0.14}$ Octahedra/C	1.92	5.16	*J. Am. Chem. Soc.* 2017, 139, 9576
Pt_3Cu icosahedra	0.736	2.14	*ACS Nano* 2015, 9, 7634
np-HEA(AlNiCuPtPdAu)	**2.25**	**3.20**	**This work**